Mon. Not. R. Astron. Soc. **000**, 1–6 (2002) Printed 12 February 2015 (MN LATEX style file v2.2)

Cross-Correlation of CFHTLenS Galaxy Number Density and Planck CMB Lensing

Y. Omori[1⋆] and G. Holder[1]
[1]*McGill University, QC, Canada, H3A2T8*

12 February 2015

ABSTRACT

We measure the cross-power spectrum between galaxy density from Canada-France-Hawaii-Telescope Lensing Survey (CFHTLenS) catalogues and gravitational lensing convergence from Planck data release 1 (2013) and 2 (2015). We investigate three main galaxy samples: $18.0 < i_{\rm AB} < 22.0$, $18.0 < i_{\rm AB} < 23.0$, $18.0 < i_{\rm AB} < 24.0$ in the redshift range $0.2 < z < 1.3$ in each of the four CFHTLenS wide fields. By comparing the measured cross-spectrum with model predictions, linear galaxy-dark matter biases of $b = 0.82^{+0.24}_{-0.23}, 0.83^{+0.19}_{-0.18}, 0.82^{+0.16}_{-0.14}$ are inferred at significances of $3.5, 4.5, 5.6\sigma$ using the Planck 2015 release. These measurements are marginally consistent with biases derived from galaxy-galaxy auto-correlations: $b = 1.15^{+0.02}_{-0.01}, 1.08^{+0.01}_{-0.01}$ and $0.96^{+0.01}_{-0.01}$ respectively. Using the 2013 Planck release, we obtain biases of $b = 1.33^{+0.29}_{-0.28}, 1.19^{+0.23}_{-0.23}, 1.16^{+0.19}_{-0.18}$, showing significant differences between the releases.

Key words: weak lensing – galaxies.

1 INTRODUCTION

An approach to measuring the distribution of dark matter in our Universe is by using weak gravitational lensing, where light is deflected by mass between the source and the observer. In the case of cosmic microwave background (CMB) weak lensing, the paths of photons emitted from the last scattering surface become perturbed by the large-scale structure in the Universe amidst their journey to the observer. This changes the statistics of hot/cold spots size distribution, leading to a change in the local angular power spectrum on the scale of the primary acoustic peaks. (Lewis & Challinor 2006). Since the degree of deflection is proportional to the integrated potential that the photon traverses, weak lensing is a sensitive probe for studying the large-scale structure between the CMB and us.

The clustering properties and statistics of dark matter halos have been extensively studied through simulations (Boylan-Kolchin et al. 2009; Klypin et al. 2011). Since these dark matter halos form in peaks in the peaks of the background density distribution, they are clustered more strongly than the background matter distribution (Kaiser 1984; Bardeen et al. 1986). Although galaxies live inside dark matter halos, the formation processes and their dynamics make the distribution of galaxies non-local and possibly stochastic relative to the halo center, making the clustering characteristics different (Mo & van den Bosch & White 2010). The ratio between the clustering amplitude of dark matter and galaxies is called linear galaxy bias.

Here we cross-correlate the galaxy number density from the Canada-France-Hawaii Telescope Lensing Survey (CFHTLenS) (Heymans et al. 2012; Erben et al. 2013; Velander et al. 2014) and the all-sky convergence map from Planck (Planck XV 2015, hereafter PXV2015) to measure galaxy biases. Similar studies include Planck lensing cross-correlated with NRAO VLA Sky Survey (NVSS) galaxies, MaxBCG clusters, SDSS LRGs and WISE (Planck XVII 2013, hereafter PXVII2013), Wilkinson Microwave Anisotropy Probe (WMAP) lensing cross-correlated with NVSS galaxies (Smith, Zahn & Doré 2007), WMAP lensing cross-correlated with LRGs and quasar from SDSS (Hirata et al. 2008) Blanco Cosmology Survey (BCS) galaxies cross-correlated with South Pole Telescope (SPT) lensing (Bleem et al. 2012), Sloan Digital Sky Survey (SDSS) quasar maps cross-correlated with Atacama Cosmology Telescope (ACT) lensing (Sherwin et al. 2012), Wide-field Infrared Survey Explorer (WISE) selected quasars cross-correlated with SPT lensing (Geach et al. 2013), Herschel/SPIRE cosmic infrared background (CIB) cross-correlated with SPT lensing (Holder et al. 2013), SPTpol E-mode polarization cross-correlated with estimates of the lensing potential from Herschel/SPIRE CIB (Hanson et al. 2013), Polarbear experiment CMB polarization cross-correlated with Herschel/SPIRE CIB (Polarbear collaboration 2014) and reconstructed convergence from ACTpol cross-correlated with CIB measurements from Planck (van Engelen et al. 2014b).

⋆ E-mail:yomori@physics.mcgill.ca

In our study, we present both the cross-correlations between galaxy overdensity and lensing, and the galaxy auto-correlations using the *same* galaxy data, and compare the linear galaxy biases that we obtain.

In this paper we assume flat ΛCDM cosmology ($\Omega_m = 0.28$, $\Omega_\Lambda = 0.72$, $H_0 = 100h$ km s^{-1}Mpc^{-1} and $\sigma_8 = 0.82$, $n_s = 0.96$) with $h = 0.70$. All magnitudes are given in the AB system.

2 THEORY

CMB lensing convergence is calculated by integrating the matter fluctuation in the line-of-sight direction:

$$\kappa(\hat{\mathbf{n}}) = \int d\chi W^\kappa(\chi)\delta[\chi\hat{\mathbf{n}}, z(\chi)], \quad (1)$$

where $\hat{\mathbf{n}}$ is the line-of-sight direction, χ is the line-of-sight comoving distance, δ is the fractional dark matter density fluctuation and W^κ is the lensing kernel:

$$W^\kappa(\chi) = \frac{3}{2}\Omega_{\rm m,0}\left(\frac{H_0}{c}\right)^2 \frac{\chi}{a(\chi)}\frac{\chi_{\rm CMB}-\chi}{\chi_{\rm CMB}}, \quad (2)$$

which describes the efficiency of lensing at a given redshift when multiplied by $d\chi/dz$.

Under the assumption of the galaxy distribution tracing out the peaks of dark matter density fluctuations, the overdensity of galaxies can be described as:

$$g(\hat{\mathbf{n}}) = \int d\chi W^g(\chi)\delta[\chi\hat{\mathbf{n}}, z(\chi)]. \quad (3)$$

The distance kernel W^g(Sherwin et al. 2012):

$$W^g(\chi) = \frac{1}{\left[\int dz' \frac{dN(z')}{dz'}\right]}\frac{dz}{d\chi}\frac{dN(z)}{dz}b(\chi) + MB(\chi) \quad (4)$$

describes the distribution of galaxies as a function of redshift in terms of co-moving distances. The second term in equation 4 is the magnification bias, where the observed number density of galaxies are altered due to lensing caused by mass between the foreground galaxy and the observer (Turner & Ostriker & Gott 1984) is given by:

$$MB(\chi) = \frac{3}{2}\Omega_{\rm m,0}\frac{c}{H(z(\chi))}\left(\frac{H_0}{c}\right)^2 (1+z(\chi))g(\chi)\,(5s-2)\,, \quad (5)$$

with

$$g(\chi) = \chi\int_\chi^{\chi_{\rm CMB}} d\chi' \frac{\chi'-\chi}{\chi'}\frac{dN/dz}{\int dz'\, dN/dz'}\frac{dz}{d\chi'}, \quad (6)$$

and

$$s = \frac{d\log_{10}N(<m)}{dm}\Big|_{m_{\rm lim}}, \quad (7)$$

for a galaxy sample with limiting magnitude $m_{\rm lim}$ (Villumsen 1995). As shown in figure 1, the amplitudes of the magnification biases for each sample are significantly smaller than the dN/dz term.

The cross-spectrum between convergence and galaxy overdensity under the Limber approximation is the power spectrum weighted by the lensing and galaxy kernels (Limber 1953; Kaiser 1992):

$$C_\ell^{\kappa g} = \int dz \frac{d\chi}{dz}\frac{1}{\chi^2}W^\kappa(\chi)W^g(\chi)P\left(k=\frac{\ell}{\chi}, z\right), \quad (8)$$

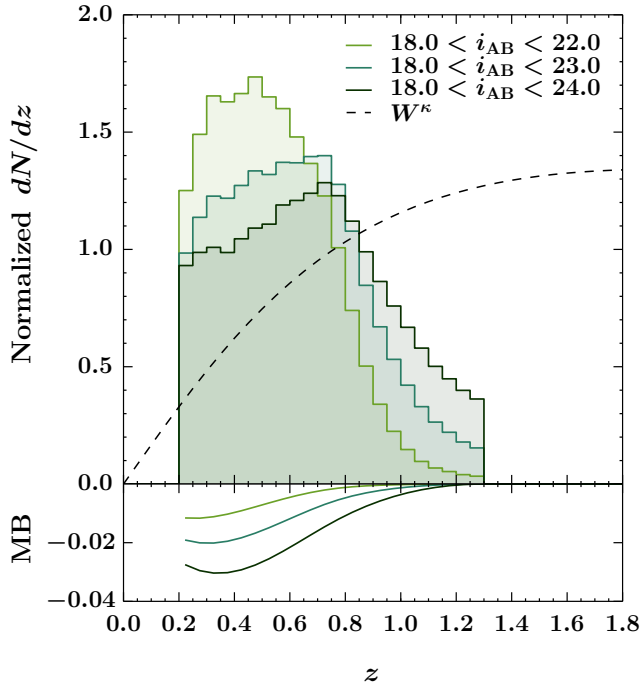

Figure 1. Light green, Turquoise, Dark green: Redshift distribution dn/dz for the $18.0 < i_{\rm AB} < 22.0$, $18.0 < i_{\rm AB} < 23.0$, $18.0 < i_{\rm AB} < 24.0$ samples in the range $0.2 < z < 1.3$. The distribution is normalized such that the integral $\int dz(dN/dz) = 1$. **Dashed line:** Convergence kernel W^κ multiplied with $(d\chi/dz)$ and arbitrary normalization applied for visualization purposes to demonstrate the effectiveness of the lenses at various redshifts. **Lower panel:** Amplitude of magnification bias for each of the galaxy samples.

where $P(k, z)$ is the non-linear matter power spectrum at redshift z. As a comparison, we also compute the galaxy overdensity auto-spectrum given by:

$$C_\ell^{gg} = \int dz \frac{d\chi}{dz}\frac{1}{\chi^2}W^g(\chi)^2 P\left(k=\frac{\ell}{\chi}, z\right). \quad (9)$$

The model spectra in equations 8, 9 are computed using the non-linear power spectrum from `CAMB` (Lewis & Bridle 2002) and revised `Halofit` (Smith et al. 2003; Takahashi et al. 2012). The redshift distributions dN/dz for each subsample are produced by averaging the individual photometric redshift probability distributions for each galaxy rather than simply using the best-fit estimates for each galaxy.

3 GALAXY MAPS

In this study, we use the galaxies from the CFHTLenS[1] galaxy survey. CFHTLenS is part of the wide component of the Canada-France-Hawaii Telescope Legacy Survey [2] (CFHTLS), which consists of 4 fields centered at 2:18:00 -07:00:00, 08:57:49 -03:19:00, 14:17:54 +54:30:31, 22:13:18 +01:19:00, each ranging from $23 - 64$ deg^2 with a total of

[1] http://cfhtlens.org/
[2] http://www.cfht.hawaii.edu/Science/CFHTLS/

154 deg^2 and full multi-colour depth of $i_{\rm AB} = 24.7$ (Heymans et al. 2012; Erben et al. 2013; Velander et al. 2014). We limit our analysis to galaxies in the redshift range $0.2 < z < 1.3$, which is confirmed by Heymans et al. (2012) to have a photometric redshift distribution that resembles the measured spectroscopic redshift distribution. Galaxies selected with $i_{\rm AB} < 24.5$ in this redshift slice have a scatter of $0.03 < \sigma_{\Delta z} < 0.06$ (where $\sigma^2_{\Delta z}$ is the variance in the difference between the photometric and spectroscopic redshifts $(z_{\rm p} - z_{\rm s})/(1 + z_{\rm s})$) with 10% of the galaxies classified as outliers (Hildebrandt et al. 2007; Benjamin et al. 2013). Within this redshift slice, three samples with $18.0 < i_{\rm AB} < 22.0$, $18.0 < i_{\rm AB} < 23.0$, $18.0 < i_{\rm AB} < 24.0$ are extracted, resulting in galaxy catalogues with mean number densities $n = 3.4, 7.7, 15.4$ per square arcminute respectively. The lower magnitude cut is applied to reduce dispersion and bias due to photometric redshift estimates in addition to removal of possible stars that passed through initial reduction pipeline classifications (`star_flag` $= 0$ and `mask` $= 0$, descriptions of each flag can be found in Erben et al. (2013)).

Using these catalogues, the fractional galaxy overdensity maps at arcminute resolution are produced by:

$$\delta_{ij} = \frac{N_{ij} - \langle N \rangle w_{ij}}{\langle N \rangle w_{ij}}, \tag{10}$$

for each i-th and j-th pixel, where w_{ij} is the pixel-by-pixel weight map produced by degrading the arcsecond resolution masks to match the same resolution and

$$\langle N \rangle = \frac{\sum_{ij} N_{ij}}{\sum_{ij} w_{ij}}. \tag{11}$$

4 CONVERGENCE MAPS

We use the observed and simulated convergence maps from the Planck 2015 release[3] (PXV2015) and compare the results with the 2013 release[4] (PXVII2013). The 2015 convergence map is produced by applying a quadratic estimator (Okamoto & Hu 2003) on a SMICA component separated map, which is synthesized by cleaning the foregrounds and combining all nine frequency bands. The Galaxy and point sources are masked in the process and the bands are restricted in the range of $100 \leq \ell \leq 2048$ (PXV2015). The 2013 map is released as a $\bar{\phi}$ map is generated by combining the 143 and 217 GHz channels with dust distribution subtracted using the 857 GHz channel. The map also masks point sources included in the ERCSC, SZ and PCCS catalogs (PXVII2013). The map is transformed into a convergence κ map by taking the transform:

$$\kappa(\boldsymbol{\ell}) = \frac{\ell(\ell+1)}{2} (\mathcal{R}^{\phi}_{\ell})^{-1} \bar{\phi}(\boldsymbol{\ell}), \tag{12}$$

where $\mathcal{R}^{\phi}_{\ell}$ is a normalization factor. We combine the Planck 2013 and 2015 masks and apply this to both convergence maps for consistency. Additional masking is not applied beyond the masks released by the Planck collaboration. Field regions were extracted by multiplying this all-sky mask with galaxy catalogue masks.

Biases in the lensing reconstruction due to the thermal Sunyaev-Zeldovich (tSZ) effect or cosmic infra-red background (CIB) fluctuations are expected to be small with Planck's angular resolution (van Engelen et al. 2014a; Osborne, Hanson & Doré 2014).

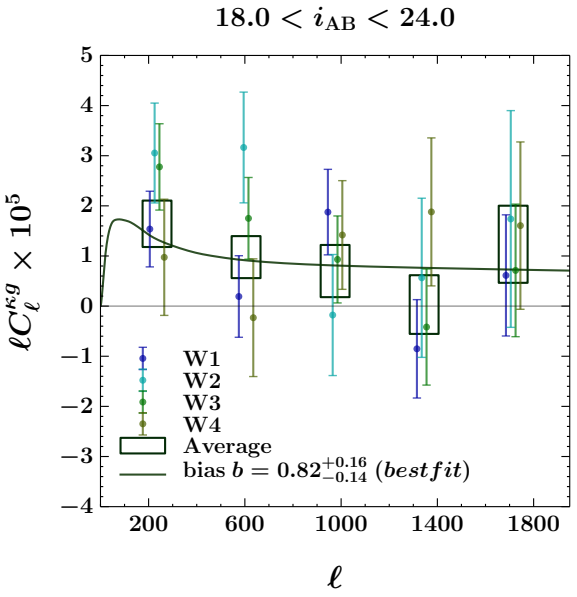

Figure 2. Cross-correlation of $18.0 < i_{\rm AB} < 24.0$ sample for W1,W2,W3,W4, and the average of the four fields with the best fit theory model.

5 CROSS AND AUTO-SPECTRUM

The cross-power spectrum is calculated using the flat-sky approximation and multiplying the maps in Fourier space:

$$C^{\kappa g}_{\ell} = f \langle Re((\mathcal{K}(\mathbf{l}) - \langle \mathcal{K}_{\rm sim}(\mathbf{l}) \rangle)^* \mathcal{G}(\mathbf{l})) \rangle |_{\mathbf{l} \in \ell} \tag{13}$$

where f is the normalization factor $N_1 N_2 / \sum w_{ij}$ and $\mathcal{K}$, $\mathcal{G}$ are the Fourier transforms of the convergence and the galaxy overdensity maps multiplied with the weight map. The auto-spectrum is calculated in a similar way but replacing $\mathcal{G}$ with $\mathcal{K}$ and subtracting the shot noise contribution $C^{\rm shot}_{\ell} = 1/\langle n \rangle$, where $\langle n \rangle$ is the average number density of galaxies per steradian.

Uncertainties are calculated by cross-correlating the galaxy maps with 100 simulated Planck convergence maps (released by the Planck collaboration) reduced through the same pipeline, and calculating the variance for each bin. Using these uncertainties, the weighted averages for each individual bin are calculated.

Since the uncertainties in the galaxy auto-spectrum cannot be derived in the same way, we resort to an internal block-jackknife method often used in 2-point correlation function analysis, where we divide each of the fields into 64 sub-regions and the jackknife samples are then created by omitting each of these sub-samples (Zehavi et al. 2005; Norberg et al. 2009). The covariance matrix is estimated by:

[3] http://irsa.ipac.caltech.edu/data/Planck/release_2/all-sky-maps/maps/component-maps/lensing/COM_CompMap_Lensing_2048_R2.00.tar

[4] http://irsa.ipac.caltech.edu/data/Planck/release_1/all-sky-maps/previews/COM_CompMap_Lensing_2048_R1.10/index.html

$$\Sigma^{gg} = \frac{N_{\rm sub}-1}{N_{\rm sub}} \sum_{n=1}^{N_{\rm sub}} (C_\ell^n - \langle C_\ell \rangle)_i (C_\ell^n - \langle C_\ell \rangle)_j, \quad (14)$$

while the covariance matrix for the cross-correlation is calculated by:

$$\Sigma^{\kappa g} = \frac{1}{N_{\rm maps}} \sum_{m=1}^{N_{\rm maps}} (C_\ell^m - \langle C_\ell \rangle)_i (C_\ell^m - \langle C_\ell \rangle)_j. \quad (15)$$

Using these covariance matricies, the best fit biases are derived by minimizing the χ^2:

$$\chi^2 = \sum_{ij} (C^X_{\ell-th} - C^X_\ell)_i (\Sigma^X)^{-1}_{ij} (C^X_{\ell-th} - C^X_\ell)_j, \quad (16)$$

where $X = \kappa g$ or gg and i, j are the bin numbers. The significance of detection is defined by $\Delta\chi^2 = \chi^2(b=0) - \chi^2_{\rm min}(b)$.

6 RESULTS

The cross-spectra for each of the fields using the $18.0 < i_{\rm AB} < 24.0$ sample are shown in figure 2, and the different magnitude samples are shown in figure 3. The best fit values b and their associated χ^2 values are listed in table 1, where the χ^2 values were calculated using 20 bins in the range of $\ell = 50 - 1900$.

The best fit biases for the Planck 2015 release are found to be $b = 0.82^{+0.24}_{-0.23}, 0.83^{+0.19}_{-0.18}, 0.82^{+0.16}_{-0.14}$ at significances of $3.5, 4.5, 5.6\sigma$ respectively. The minimum χ^2 for the fits are 25.4, 18.6, 15.0 with a probability-to-exceed (PTE) of 0.15, 0.48, and 0.72. These best fit biases are significantly lower than the biases found from the Planck 2013 release: $b = 1.33^{+0.29}_{-0.28}, 1.19^{+0.23}_{-0.23}, 1.16^{+0.19}_{-0.18}$. Similarly, the best fit biases from C_ℓ^{gg} are found to be $1.15^{+0.02}_{-0.01}, 1.08^{+0.01}_{-0.01}, 0.96^{+0.01}_{-0.01}$, with χ^2 of 14.1, 22.1, 38.0. Sample correlation matricies are shown in figure 4.

These results suggest that unlike quasars, which are strongly biased tracers of dark matter (see Geach et al. 2012, Sherwin et al. 2012), optically-selected galaxies in these magnitude ranges on average are *unbiased* tracers of dark matter fluctuations.

7 CONCLUSION

We have presented the results of cross-correlations between galaxy number density from CFHTLenS and CMB lensing convergence from Planck, along with galaxy-galaxy auto-correlations. We obtain the dark matter-galaxy bias using these two *independent* methods. For the cross-correlations of the 3 magnitude samples, we obtain best fit biases of $b = 0.82^{+0.24}_{-0.23}, 0.83^{+0.19}_{-0.18}, 0.82^{+0.16}_{-0.14}$ in the range of $50 < \ell < 1900$ using the 2015 release and $b = 1.33^{+0.29}_{-0.28}, 1.19^{+0.23}_{-0.23}, 1.16^{+0.19}_{-0.18}$ using the 2013 release. From the galaxy auto-correlations, we obtain biases of $b = 1.15^{+0.02}_{-0.01}, 1.08^{+0.01}_{-0.01}, 0.96^{+0.01}_{-0.01}$, which settle between the values obtained from the two data releases and agrees well with previously established results that indicate linear galaxy bias of $\simeq 1$ at large scales (see for example Gaztanaga & Frieman 1994).

Although the galaxy-galaxy auto-correlations place stronger constraints on the value of the bias, these cross-correlations provide a more direct measurement of the relationship between galaxies and two-dimensional projected mass, because the degree of photon path deflection is directly correlated with the depths of foreground gravitational potentials that it passes through. Furthermore, cross-correlations are less sensitive to the complexity of survey masks and any hidden systematic errors that could be present in any single survey.

The power of cross-correlations is yet to be used at full potential. With the advent of upcoming wide galaxy surveys probing to fainter magnitudes, the sky coverage will improve the statistics while the depth will provide sufficient galaxy number density to maintain signal above shot-noise. For example, similar cross-correlation analyses will be performed between the Dark Energy Survey (DES) galaxies - SPT/SPTpol lensing and Hyper Supreme Camera (HSC) survey galaxies - ACT/ACTpol lensing, which will have several thousand square degrees of overlap. With such large areas and fainter magnitude limits, the signal to noise is expected to be an order of magnitude larger.

8 ACKNOWLEDGEMENTS

The authors thank Ludovic Van Waerbeke, Joachim Harnois-Déraps and Duncan Hanson for helpful discussions and valuable comments on the manuscript. This work is based on observations obtained with MegaPrime/MegaCam, a joint project of CFHT and CEA/DAPNIA, at the Canada-France-Hawaii Telescope (CFHT) which is operated by the National Research Council (NRC) of Canada, the Institut National des Sciences de l'Univers of the Centre National de la Recherche Scientifique (CNRS) of France, and the University of Hawaii. This research used the facilities of the Canadian Astronomy Data Centre operated by the National Research Council of Canada with the support of the Canadian Space Agency. CFHTLenS data processing was made possible thanks to significant computing support from the NSERC Research Tools and Instruments grant program. Some of the results in this paper have been derived using the HEALPix Górski et al. (2005) package.

REFERENCES

Bardeen J. M., Bond J. R., Kaiser N., Szalay A.S., 1986, ApJ, 304, 15
Benjamin J. et al., 2013, MNRAS, 431, 1547
Bleem L.E. et al., 2012, ApJ, 753, 9
Boylan-Kolchin M., Springel V., White S. D. M. and Jenkins A., Lemson G., 2009, MNRAS, 398, 1150-1164
Erben T et al., 2013, MNRAS, 433
Gaztanaga E., Frieman J. A., 1994, ApJ, 437, L13
Geach J.E. et al., 2013, ApJ, 776, L41
Górski K. M et al., 2005, ApJ, 622, 759
Hanson D. et al., 2013, Phys. Rev. Lett., 111, 14
Heymans C. et al., 2012, MNRAS, 427, 146
Hirata C. M. et al., 2008, Phys. Rev. Lett., 78, 4
Holder G. P et al., 2013, ApJ, 771, L16
Hildebrandt H. et al., 2012, MNRAS, 421, 2355
Kaiser N., 1984, ApJ, 284, L9

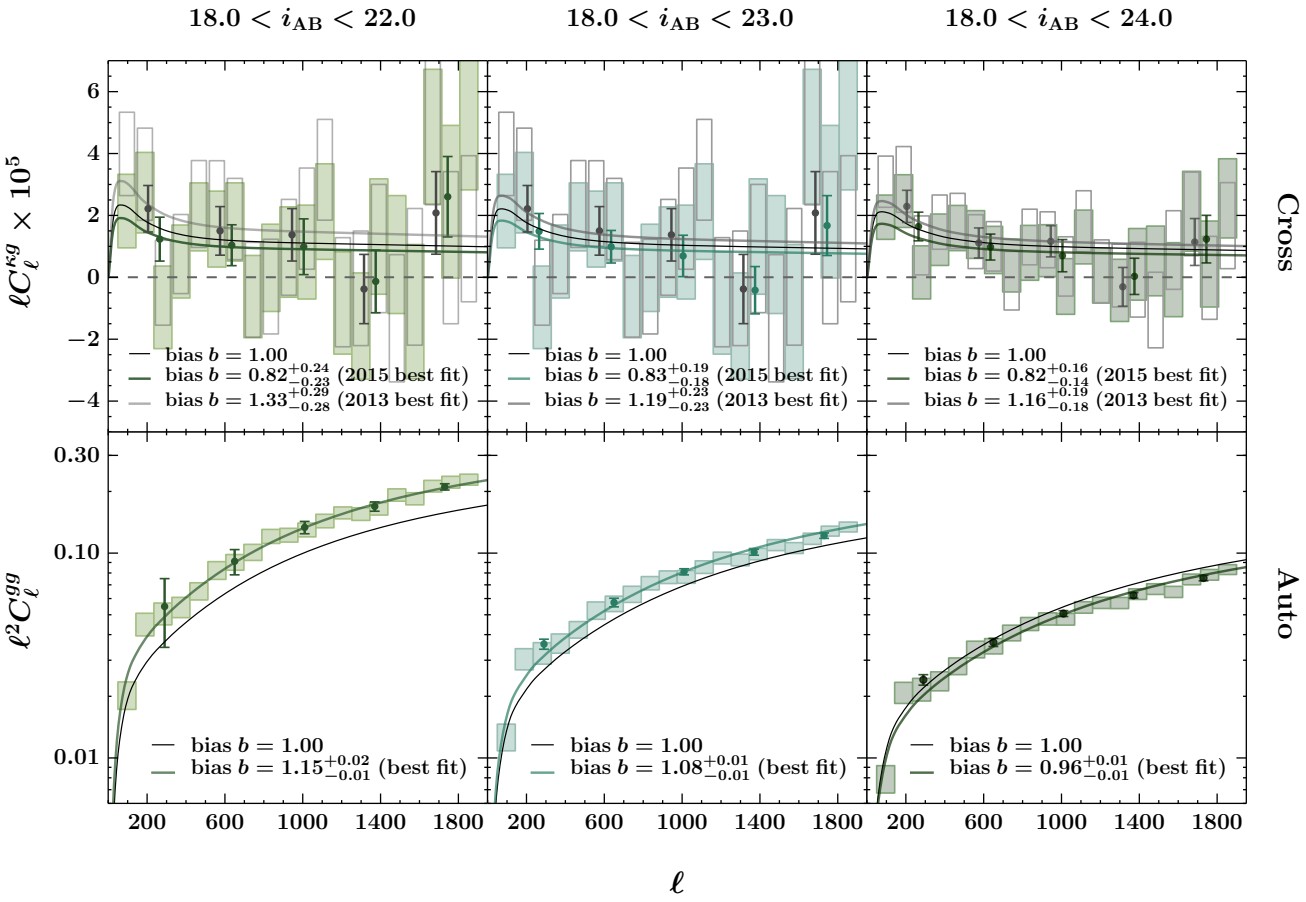

Figure 3. Cross-spectrum $C_\ell^{\kappa g}$ for the $18.0 < i_{\rm AB} < 22.0$, $18.0 < i_{\rm AB} < 23.0$, $18.0 < i_{\rm AB} < 24.0$ galaxy samples cross-correlated with Planck convergence (filled bars: 2015, empty bars: 2013) (upper row) and the auto-spectrum using the same galaxy samples (lower row). The points with errorbars shown are the coarsely binned calculations for displaying purposes, and the χ^2 are the fits to the 20 bins shown in the background.

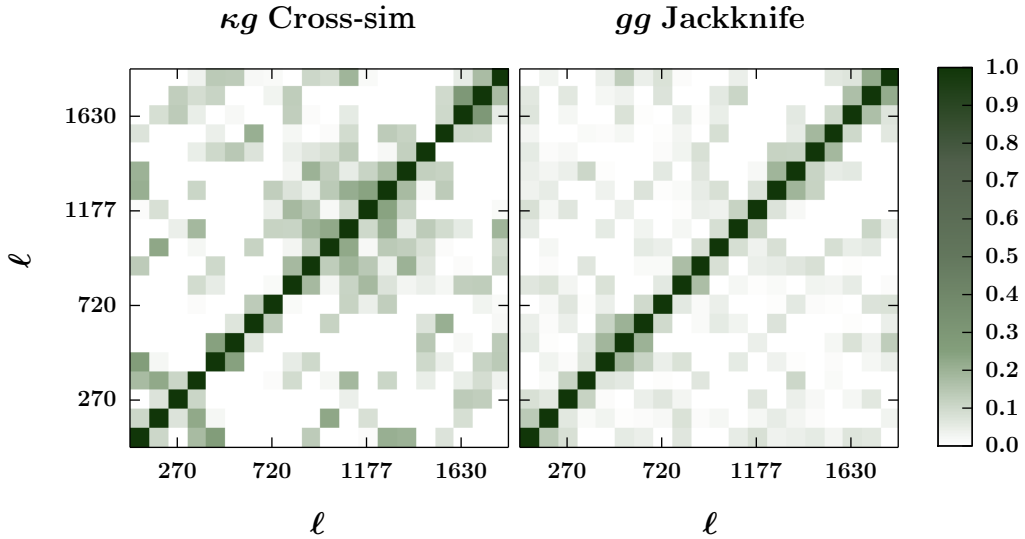

Figure 4. Correlation matrices between bins for cross-correlation and auto-correlation.

Sample	N	$\langle n \rangle$ [arcmin^{-2}]	b (C_ℓ^{gg})	χ^2	b_{2015} ($C_\ell^{\kappa g}$)	χ^2	b_{2013} ($C_\ell^{\kappa g}$)	χ^2
$18 < i_{\rm AB} < 22$	1444906	3.4	$1.15^{+0.02}_{-0.01}$	14.1	$0.82^{+0.24}_{-0.23}$	25.4	$1.33^{+0.29}_{-0.28}$	15.4
$18 < i_{\rm AB} < 23$	3268383	7.7	$1.08^{+0.01}_{-0.01}$	22.1	$0.83^{+0.19}_{-0.18}$	18.6	$1.19^{+0.23}_{-0.23}$	15.9
$18 < i_{\rm AB} < 24$	6529185	15.4	$0.96^{+0.01}_{-0.01}$	38.0	$0.82^{+0.16}_{-0.14}$	15.0	$1.16^{+0.19}_{-0.18}$	15.4

Table 1. Table of best fit linear bias and χ^2 values calculated using 20 bins between $50 < \ell < 1900$.

Kaiser N., 1992, ApJ, 388, 272
Klypin A. A., Trujillo-Gomez S., Primack J., 2011, ApJ, 740, 102
Limber D. N., 1953, ApJ, 117, 134
Lewis A., Bridle S., 2002, Phys. Rev. D, 66, 103511
Lewis A., Challinor A., 2006, Phys. Rep., 429, 1-65
Mo H., van den Bosch F., White S., 2010, Galaxy Formation and Evolution, Cambridge Univ. Press
Norberg P. et al., 2009, MNRAS, 396, 19
Okamoto T., Hu. W., 2003, Phys. Rev. D. 67, 083002
Osborne S.J., Hanson D., Doré O., 2014, J. Cosmol. Astropart. Phys., 3, 24
Planck Collaboration XVII, 2013, A & A, 571, A71
Planck Collaboration XV, 2015, preprint (arXiv:1303.5077)
Polarbear collaboration et al., 2014, Phys. Rev. Lett., 112, 13
Sherwin B. D. et al., 2012, ApJ, 86, 8
Smith R. E. et al. [Virgo Consortium Collaboration], 2003, MNRAS, 341, 1311
Smith K. M., Zahn O., Doré O., 2007, Phys. Rev. D, 76, 043510
Takahashi R. et al., 2012, ApJ, 761, 152
Turner E. L., Ostriker J. P., Gott J. R., 1984, ApJ, 284, 1
van Engelen A. et al., 2012, ApJ, 756,142
van Engelen A. et al., 2014, ApJ, 786, 13
van Engelen A. et al., 2014, preprint (arXiv:1412.0626)
Velander M. et al., 2014, MNRAS, 437, 2111
Villumsen, J., 1995b, astro-ph/9512001
Zehavi I. et al., 2005, ApJ, 630, 1-27